

SSF-Net: Spatial-Spectral Fusion Network with Spectral Angle Awareness for Hyperspectral Object Tracking

Hanzheng Wang[✉], Wei Li[✉], *Senior Member, IEEE*, Xiang-Gen Xia[✉], *Fellow, IEEE*, Qian Du[✉], *Fellow, IEEE*, and Jing Tian[✉], *Member, IEEE*

Abstract—Hyperspectral video (HSV) offers valuable spatial, spectral, and temporal information simultaneously, making it highly suitable for handling challenges such as background clutter and visual similarity in object tracking. However, existing methods primarily focus on band regrouping and rely on RGB trackers for feature extraction, resulting in limited exploration of spectral information and difficulties in achieving complementary representations of object features. In this paper, a spatial-spectral fusion network with spectral angle awareness (SST-Net) is proposed for hyperspectral (HS) object tracking. Firstly, to address the issue of insufficient spectral feature extraction in existing networks, a spatial-spectral feature backbone (S^2FB) is designed. With the spatial and spectral extraction branch, a joint representation of texture and spectrum is obtained. Secondly, a spectral attention fusion module (SAFM) is presented to capture the intra- and inter-modality correlation to obtain the fused features from the HS and RGB modalities. It can incorporate the visual information into the HS spectral context to form a robust representation. Thirdly, to ensure a more accurate response of the tracker to the object position, a spectral angle awareness module (SAAM) investigates the region-level spectral similarity between the template and search images during the prediction stage. Furthermore, we develop a novel spectral angle awareness loss (SAAL) to offer guidance for the SAAM based on similar regions. Finally, to obtain the robust tracking results, a weighted prediction method is considered to combine the HS and RGB predicted motions of objects to leverage the strengths of each modality. Extensive experiments on the HOTC dataset demonstrate the effectiveness of the proposed SSF-Net, compared with state-of-the-art trackers.

Index Terms—HS object tracking; Attention mechanism; Feature fusion; Spectral angle; Deep learning.

I. INTRODUCTION

VISUAL object tracking has gained significant research attention in recent years due to its applications in autonomous driving [1], human-computer interaction [2], and intelligent security [3]. It aims to follow the same object in subsequent frames based on the initial location in the first frame of a video sequence. While RGB-based trackers have

Hanzheng Wang, Wei Li, and Jing Tian are with the School of Information and Electronics, Beijing Institute of Technology, Beijing 100081, China, and also with the Beijing Key Laboratory of Fractional Signals and Systems, Beijing 100081, China (e-mail: hzwangc@bit.edu.cn; liwei089@ieee.org; tianjing@bit.edu.cn).

Xiang-Gen Xia is with the Department of Electrical and Computer Engineering, University of Delaware, Newark, DE 19716, USA (e-mail: xxia@ee.udel.edu).

Qian Du is with the Department of Electrical and Computer Engineering, Mississippi State University, Starkville, MS 39762, USA (e-mail: du@ece.msstate.edu).

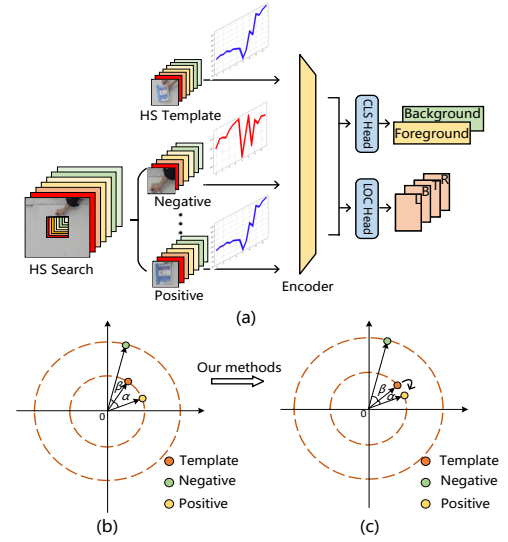


Fig. 1. Illustration of the issue in the tracking paradigm and the main idea of our methods.

been developed to handle challenging scenarios with object density, occlusions, and long-duration tracking, they rely on visual features like color and texture, which are susceptible to background clutter. In contrast, Hyperspectral video (HSV) cameras offer the advantage of capturing both visual texture information and spectral reflectance properties of object materials [4]. This means that even when the object and background have similar colors, their material characteristics are different, which can allow for the use of material spectral reflectance to distinguish the object from the background. Furthermore, with the advancements in HS imaging equipment, acquiring hyperspectral (HS) images has become more convenient, which leads to the thriving development of HS object tracking in recent years.

In the earlier studies, hand-crafted features were designed to represent the spectral information of HS data cubes [5]. Xiong *et al.* [6] considered the 3-D spatial-spectral histogram of HS images and constructed an HS object tracking dataset to validate the effectiveness of the proposed methods. Hou *et al.* [7] leveraged the correlation filters to deal with the motion prediction of objects and designed a regularizer for optimization. However, with the advancements in deep learning, hand-crafted features are gradually being replaced by more robust

convolutional features that offer improved performance and reliability.

The deep learning-based methods [8], [9] are roughly divided into two categories: band regrouping-based methods and cross-modality fusion-based methods. The former focuses on utilizing the existing RGB trackers to deal with the HS images through transfer learning. Gao *et al.* [10] proposed a feature fusion network, CBFF-Net, to fuse the information from different band groups. Li *et al.* [11] reconstructed the HS images through the auto-encoder learning to capture the intrinsic between the bands. In this way, the HS images are regrouped into multiple three-channel false-color images. However, the band regrouping-based methods just utilize the RGB trackers to extract the feature of the regrouped HS images, which neglect the relationship between spatial-spectral features. There is a lack of feature extraction networks suitable for HS images that consider both spatial and spectral characteristics simultaneously. The latter focuses on combining the advantages of RGB trackers and HS trackers. Liu *et al.* [12] designed an RGB and an HS branch to form the robust representation of the objects jointly. The RGB images and HS images from the same scenario are input to the network to predict the subsequent motions of the objects. Zhao *et al.* [13] proposed a fusion network based on the Transformer encoder and the robust tracking results are obtained from RGB and HS streams through the self-attention mechanism. Despite these advancements, the impact of various modality fusion methods is not yet fully understood, and there remains a gap in the development of effective feature-level fusion methods for HS object tracking.

Moreover, HS trackers often adopt the RGB tracking framework, which comprises a classification (CLS) head and a localization (LOC) head. However, this approach does not fully exploit the rich multi-spectral information available in HS data, leading to sub-optimal robustness in tracking performance. As depicted in Figure 1(a), the conventional tracking paradigm creates a shared feature space through encoder embeddings. The CLS and LOC heads then predict the class and location of objects respectively, utilizing depth-wise correlation computations such as generalized Euclidean or cosine metrics—yet they do not account for the spectral correlation between HS template images (TI) and HS search images (SI). As illustrated in Figure 1(b), for a trained HS tracker, although the classification and location loss converges, the included angles α of the TI and positive SI and β of the TI and negative SI are uncertain. The included angles of negative pairs may be larger than positive pairs [14]. This problem makes the tracker unable to deal with the disturbance from similar negative objects. Thus, it is necessary to constrain the included angles of both of the above pairs in the common feature space, as shown in Figure 1(c).

To address the above problems, a spatial-spectral fusion network (SSF-Net) with spectral angle awareness is proposed. Firstly, to extract robust features and facilitate cross-modality feature fusion, a novel spatial-spectral feature backbone S^2 FB especially for HS images is designed, which includes several spatial-spectral convolution blocks (S^2 CB). Besides, with the downsample layers and residual connections of S^2 CB, the

high-level semantic information is captured and the subsequent features can be fused naturally. Secondly, to incorporate the visual information from the RGB modality into the HS branch, a spectral attention fusion module (SAFM) is proposed. Compared with the other fusion-based trackers, the SAFM captures the cross-spectral context within modalities, and the HS fused features are obtained from the RGB and the HS modalities in a self-adaptive way. So, sufficient visual prompts are supplemented to the HS branch. Finally, to fully exploit the relationships between bands and enhance the robustness of the tracking results, a spectral angle awareness module (SAAM) and a novel spectral angle awareness loss (SAAL) are proposed. Inspired by the spectral angle [15], the spectral similarity is determined by the angle between two feature vectors, which we believe can assist the classification branch in predicting the location. Between TI and SI, the spectral angle for the regions corresponding to positive samples should be small, whereas, for negative samples, it should be large. With the training of the SAAL, the SAAM is capable of accurately predicting the position of the object, serving as a complement to the CLS head. Moreover, to further improve performance, a weighted prediction module is utilized to integrate predictions from both RGB and HS modalities.

The main contributions of this article are as follows:

- 1) A spatial-spectral fusion network with spectral angle awareness (SST-Net) for HS object tracking is proposed, which integrates the information of the HS and RGB modalities to form the robust fusion feature representation, effectively enhancing the tracking performance.
- 2) An S^2 FB is proposed to extract HS features, instead of using the off-the-shelf RGB tracker, which aims to model the spatial and spectral context information jointly. Moreover, an SAFM is designed to combine the HS and RGB features with the intra- and cross-modality correlation modeling, thereby generating a more robust HS feature representation.
- 3) An SAAM is proposed to capture the spectral angle similarity between regions of feature maps to perceive the positions of objects precisely. With the guidance of SAAL, the SAAM can focus on the similar regions between TI and SI. Extensive experiments on the public dataset show the effectiveness of our proposed methods.

The remaining structure of the paper is organized as follows. Section II reviews the related works including RGB tracker, HS tracker, and fusion tracking. Section III introduces the proposed SSF-Net. Extensive ablation and comparative experimental results are shown in Section IV to show the effectiveness of the proposed methods on the HOTC datasets. Finally, Section V concludes the article.

II. RELATED WORK

A. Visual Object Tracker

The existing research on RGB trackers is roughly divided into two categories: trackers based on Siamese networks and trackers based on Transformers. On one hand, the Siamese network was originally proposed by SiamFC [16], which extracts features from query images and template images

for similarity matching. After that, many works [17], [18] focus on extracting discriminative features and improving the robustness of tracking performance. Li *et al.* [19] incorporated the region proposal network into the Siamese tracker and the tracking problem is considered as a one-shot detection task. Guo *et al.* [20] proposed a graph attention sub-network to propagate the object information from TI to SI. With the graph attention mechanism, the object structure and part-level information can be considered. Chen *et al.* [21] proposed a general framework SiamBAN to simplify the complex anchor calculations. It is a unified fully convolutional network that directly predicts the category and location of objects, avoiding the anchor configurations. On the other hand, due to the excellent ability in modeling the correlation of self-attention mechanism, the Transformer-based trackers [22], [23] have attracted more attention in recent years. Ye *et al.* [24] designed a framework named OTrack, which can extract the features and model relations of TI and SI in a unified way. Yan *et al.* [25] proposed a Transformer-based tracker, STARK, which considers the global spatial and temporal features simultaneously. Zhu *et al.* [26] proposed a multi-modality tracking paradigm based on the visual prompts. With the fine-tuning of the foundation model, the Transformer-based tracker can deal with multiple modalities of images.

B. HS Object Tracker

HS imaging, with its enhanced spectral information, offers rich spectral features, which has proven to be a powerful modality in addressing the challenge of background clutter in visual object tracking. In some early works, hand-crafted features were adopted to represent objects. Nguyer *et al.* [26] introduced a framework that utilized radiative transfer theories to estimate object reflectance. Uz Kent *et al.* [27] proposed a kernelized correlation filter (KCF) based tracker, which can track aerial vehicles using an adjustable cross-modality HS equipment. With the proposed KCF-in-multiple regions-of-interest (ROIs) approach, a reliable region prediction is obtained. Xiong *et al.* [6] proposed the material-based tracking framework to deal with the HS tracking problem. Two feature extractors are used to capture the local spectral and spatial features. Thus, the texture and spectral information can be obtained respectively. On the other hand, recent works mainly focus on using the convolutional feature to represent the object. Li *et al.* [28] proposed a band regrouping method to generate three-channel false-color images to leverage the RGB tracker to deal with the HS images. Li [29] adopted the pre-trained RGB tracker to predict raw tracking results and designed an image enhancement module to improve the image quality. Chen *et al.* [30] proposed a spectral awareness module to regroup the bands considering the spectral nonlinear interactions and the dynamic TI matching strategy generated reliable tracking results. Islam *et al.* [31] proposed a background-aware band selection method that captures the spatial changes of each band. The most important bands can be selected to generate the false-color images.

C. Fusion Tracking

Multi-modality fusion tracking, which integrates information from different modalities, has become a prominent area of focus in object tracking. One modality combination that has garnered significant attention is the fusion of RGB and infrared modalities. This approach has proven to be highly effective in enhancing tracking performance, especially in challenging conditions. Zhang *et al.* [32] proposed a discriminative model prediction tracker (DMP), which adopted a multi-level fusion mechanism and presented an object estimation network to improve the performance of RGB-T tracking. Zhang *et al.* [33] proposed an RGB-T tracker JMMAC, which considered the appearance and motion cues of objects jointly to generate reliable features. The modality fusion weights are obtained from offline-trained networks, avoiding training costs. Lan *et al.* [34] proposed a graph-based label prediction model to capture the relationship of the samples and obtain the importance weights of modalities. With the measure of modality discrimination, the model can predict robust tracking results. As for HS object tracking, the existing work has not yet given sufficient attention to this aspect. Liu *et al.* [12] proposed a fusion-based tracker SiamHYPER, which extracted both RGB and HS features. With the channel attention mechanism [35], the fused features are obtained. In the inference stage, the RGB and HS branches are used to predict the motion of objects respectively. Zhao *et al.* [13] proposed a Transformer-based network named TFTN, which captured the cross-modality and intra-modality information of different modalities.

III. PROPOSED METHOD

A. Framework Overview

The overall network structure is shown in Figure 2. Firstly, an RGB stream and an HS stream are used to extract features from the input image. To address the issue of insufficient modeling of HS images using existing methods, S^2FB is proposed for feature extraction of HS streams. The S^2FB includes the spatial-spectral convolutional block (S^2CB), which effectively captures both spatial and spectral information, resulting in more discriminative features for cross-modality fusion tracking. The RGB stream adopts the conventional Res-Net architecture and serves as a backbone network. It is worth noting that the two streams of the SSF-Net backbone network also have four stages. It can simultaneously extract features from different semantic levels, and it facilitates feature fusion with the RGB-stream backbone network at the same stage. In addition, an SAFM is proposed for spectral feature fusion of RGB-stream and HS-stream. Specifically, considering that different bands (spectra) contain different semantic information, a spectral attention network is proposed to enhance cross-modality feature representation, which flows from the backbone network to SAFM in a gating mechanism, then performs cross-modality feature fusion to obtain HS fused features. Then, to make robust tracking results, we simultaneously predict the object motions on both RGB and HS streams and adopt a weighted ensemble strategy to fuse the tracking results of the two streams. The RGB stream utilizes the tracking header of the existing object tracking framework

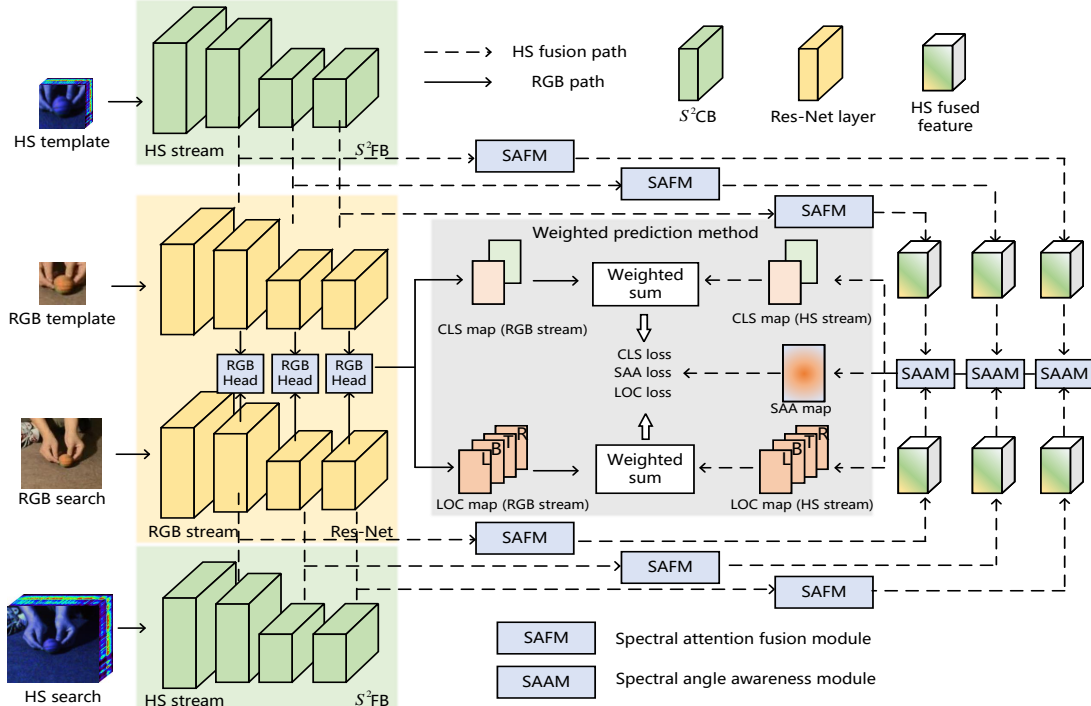


Fig. 2. Illustration of the overall structure of our proposed SSF-Net, including the bi-stream feature extraction backbone, spectral attention fusion module, spectral angle awareness module, and the weighted prediction method.

[21], thus the classification and location maps can be obtained. For the HS stream, the SAAM is proposed, which consists of a spectral angle awareness branch, along with classification and localization branches. Inspired by spectral angle mapping [15], this module calculates the similarity between spectra by measuring the angle between spectral feature vectors. By comparing spectral angles between different regions, the tracker can identify similar regions between two frames. Finally, to effectively train the network, the SAAL is proposed to increase the predicted spectral similarity between the TI and object regions of SI and lead the tracker to focus on the similar regions between TI and SI. After that, the SAAL is combined with classification loss and location loss for multi-task training of the network, which ensures that the network learns to effectively utilize spectral information for accurate tracking.

B. Bi-stream Feature Extraction Backbone

To extract the robust features, a bi-stream feature extraction backbone is proposed, which consists of the HS stream and the RGB stream. Most existing HS tracking methods utilized the off-the-shelf models in the RGB domain, such as VGG, ResNet, etc, to extract the HS features. However, HS images constitute a data cube enriched with information across numerous spectral bands, which can offer a wealth of multidimensional information, and the backbone network pre-trained from three-channel RGB images is insufficient to extract robust spatial-spectral features.

Thus, we propose a feature extraction backbone S^2FB for HS-stream. Its main structure is shown in the Figure 3. The

size of input images is $H \times W \times B$, where H and W denote the height and width of the input images, and B denotes the number of spectral bands. The S^2FB consists of four feature extraction stages. Each stage captures different feature responses to the input data. In the early stages, the network focuses on capturing details and local features, while in the later stages, as the network deepens, it captures higher-level semantic information. So, S^2FB can extract discriminative features across multiple layers, ranging from shallow to deep. The first two stages, which are referred to as “Stage 1” and “Stage 2”, include S^2CB and downsampling layers. The purpose of these stages is to ensure that the feature size is compatible with the RGB stream for feature fusion and to capture texture information. The output resolutions of these stages are $\frac{H}{2} \times \frac{W}{2} \times C$ and $\frac{H}{4} \times \frac{W}{4} \times 2C$, respectively. C denotes a channel dimension, which equals 256 in the SSF-Net. The subsequent stages, Stage 3 and Stage 4, repeat the process without downsampling and produce output with the resolutions of $\frac{H}{4} \times \frac{W}{4} \times 4C$ and $\frac{H}{4} \times \frac{W}{4} \times 8C$, respectively. Each S^2CB within the stages consists of two S^2C layers, along with batch normalization (BN) and ReLU activation layers. As shown in Figure 3, the S^2C layer utilizes 2-D depth-wise separable convolution to extract spatial features and 3-D convolution to extract multi-spectrum features. The sliding 3-D convolutional kernels establish contextual relationships between multiple continuous spectral bands and capture spectral signatures of substances. This allows the S^2CB to generate a joint spatial-spectral hierarchical representation. Additionally, the use of skip connections in the S^2CB helps mitigate issues such as vanishing gradients and facilitates information flow across

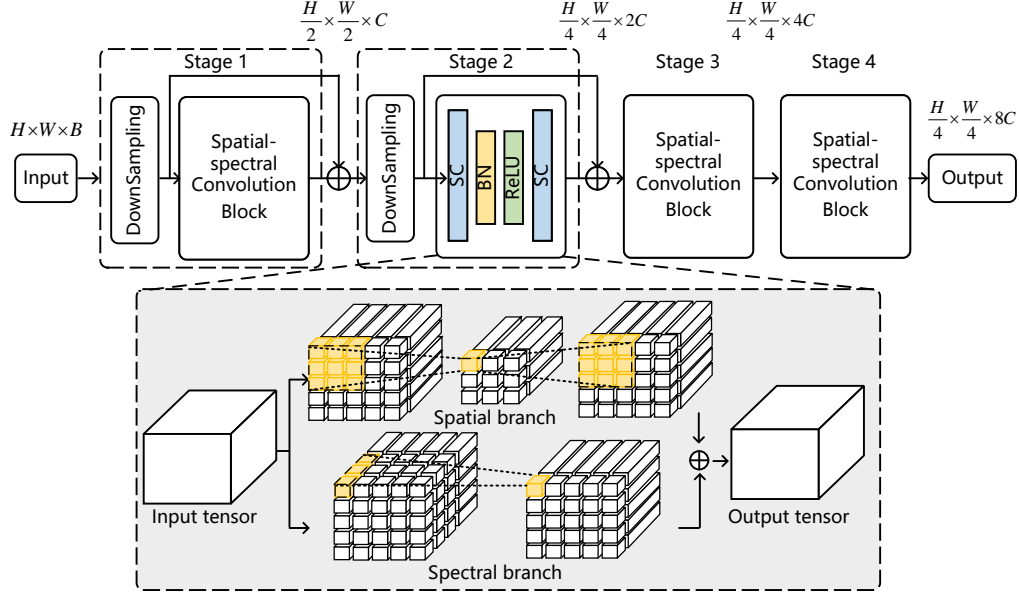


Fig. 3. Illustration of our proposed S^2FB . It consists of several S^2CB with the residual connection.

different layers. In the RGB branch of our network, we utilize ResNet-50 as the feature extraction backbone. This backbone is pre-trained on RGB tracking datasets, specifically those used in the Siamese tracking framework proposed by Chen *et al.* [21]. By leveraging the pre-trained knowledge in the RGB domain, we can transfer this knowledge to the task of HS and RGB fusion tracking. This allows us to benefit from the expertise and insights gained from previous research in RGB tracking, and enhance the performance and effectiveness of our proposed network.

C. Spectral Attention Fusion Module

Fusion tracking has been proven to be an effective method for leveraging the unique characteristics of both HS and RGB data. By combining the detailed visual texture information from RGB imagery with the rich spectral information from HS data, fusion trackers can achieve superior performance. However, existing methods often fail to adequately adjust spectral information during feature fusion, and they also lack comprehensive modeling of dependency relationships between spectral channels. Therefore, an SAFM is proposed to enable more refined adjustments for spectral information during feature fusion. By incorporating a channel attention mechanism, the SAFM allows for a weighted fusion of features from the two modalities, which ensures that the spectral information is appropriately considered.

In recent HS object tracking methods, feature fusion has been achieved through a spectral attention mechanism. However, most of the feature refinement is carried out within modalities, without fully considering the cross-modality interaction relationships and the complementary nature of modality features. To address these limitations, SAFM is proposed for cross-modality feature fusion, while modeling the feature relationships within and between modalities. As shown in

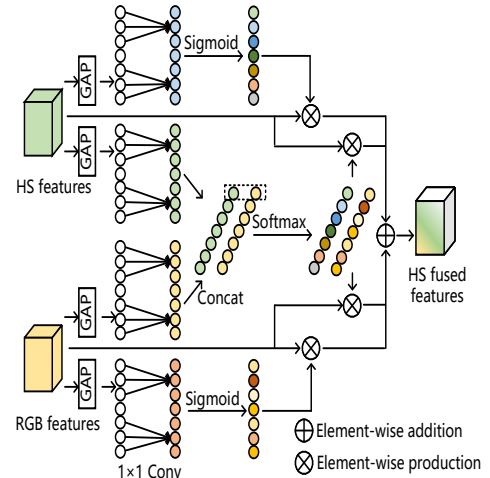


Fig. 4. The architecture of the SAFM. It consists of a global average pooling layer to generate the feature vectors, and several 1×1 convolution layers to obtain the cross-modality and intra-modality attention weights.

Figure 4, a global average pooling is first used to aggregate the spatial information into a channel-wise global feature, which is useful for capturing the overall presence of features in the input features. Assuming that $R_f \in \mathbb{R}^{H \times W \times C}$ and $H_f \in \mathbb{R}^{H \times W \times C}$ are the extracted features from RGB and HS images, respectively, the global average pooling is utilized to generate features $R_a \in \mathbb{R}^{1 \times C}$ and $H_a \in \mathbb{R}^{1 \times C}$. Then, intra-modality spectral embedding and inter-modality spectral embedding are achieved through 1-D convolution with different parameters. To capture local cross-channel interaction information and account for the similarity of adjacent spectra, we fix the size of the 1-D convolutional kernel. This allows

us to effectively model the relationships between channels. It is formulated by

$$\begin{aligned} R_e^{intra} &= C1D_1(R_a), \\ H_e^{intra} &= C1D_1(H_a), \\ R_e^{inter} &= C1D_2(R_a), \\ H_e^{inter} &= C1D_2(H_a), \end{aligned} \quad (1)$$

where $C1D_1$ and $C1D_2$ denote two different 1×1 convolution layers, respectively. For the intra-modality attention, with the spectral embedding features, the spectral attention weights are obtained through the *Sigmoid* activation function, which is formulated by

$$\begin{aligned} R_W^{intra} &= \text{Sigmoid}(R_e^{intra}), \\ H_W^{intra} &= \text{Sigmoid}(H_e^{intra}). \end{aligned} \quad (2)$$

The intra-modality refined features can be obtained from the product of input features and attention weights, which are formulated by:

$$\begin{aligned} R_{refined}^{intra} &= R_W^{intra} \otimes R_f, \\ H_{refined}^{intra} &= H_W^{intra} \otimes H_f, \end{aligned} \quad (3)$$

where \otimes denotes the element-wise product. For the inter-modality attention, the RGB embedding $R_e^{inter} \in \mathbb{R}^{1 \times C}$ and HS embedding $H_e^{inter} \in \mathbb{R}^{1 \times C}$ are concatenated to form feature $E \in \mathbb{R}^{2 \times C}$, and the *Softmax* activation function is used to generate the attention weight $W \in \mathbb{R}^{2 \times C}$ of the concatenated dimension, which represents dynamic guidance of the network on multi-modality correlation relationships. It is formulated by:

$$W = \text{Softmax}(E). \quad (4)$$

Then the inter-modality refined features between the RGB and HS modalities are obtained by the following formula:

$$\begin{aligned} R_{refined}^{inter} &= W[0] \otimes R_f, \\ H_{refined}^{inter} &= W[1] \otimes H_f, \end{aligned} \quad (5)$$

where $W[0] \in \mathbb{R}^{1 \times C}$ and $W[1] \in \mathbb{R}^{1 \times C}$ denote the first and the second row vectors of W , respectively. Finally, the intra-modality and inter-modality features are added together to obtain the HS fused feature representation. As shown in Figure 2, the SAFM focuses on the last three stages of the RGB and HS backbone networks and performs feature fusion between Stages 2, 3, and 4. Finally, the HS fused feature is input to the SAAM for predicting the object motions.

D. Spectral Angle Awareness Module

This section introduces the proposed spectral angle awareness module, including the spectral angle awareness head, classification head, and localization head. The existing methods only use the classification and localization branches in the existing RGB domain, and calculate the depth-wise similarity of each feature [36] to predict the position and size of the object. They do not fully utilize the spectral information in HS and lack modeling of spectral relationships, which will affect the robustness of the features. To solve this problem, a spectral angle awareness module is proposed.

1) Spectral angle mapping revisit. The spectral angle mapping (SAM), initially introduced by [15], is a widely used measure in remote sensing [37], [38] to assess the similarity between spectral feature vectors. In the HS object detection field, SAM calculates the similarity between an object pixel and a test pixel by first calculating their corresponding mapping matrix. This matrix is then used to compute the cosine of the angle between the spectral vectors of the pixels. The cosine value serves as an effective measure of similarity, with a higher cosine indicating a closer match to the spectral signature of the objects being compared. The specific details are as follows.

Assuming that the spectral feature $\hat{S} \in \mathbb{R}^{H \times W \times C}$ extracted by machine learning algorithms is a three-dimensional data cube, which is first transformed into a two-dimensional matrix $S \in \mathbb{R}^{HW \times C}$. The original mapping matrix M is obtained by:

$$M = \frac{1}{HW} (S^T S), \quad (6)$$

which is the estimate of the second-order statistical covariance matrix of S . Then, the mapping matrix $M^{-1/2}$ is obtained by:

$$M^{-1/2} = QV^{-1/2}Q, \quad (7)$$

where Q is an orthogonal identity matrix, and V is the eigenvalue diagonal matrix of M . With the mapping matrix $M^{-1/2}$, the spectrum t of an object and sparse tensor S are projected into the same subspace. The cosine similarity is formulated as:

$$\cos_{(i,j)}^{\wedge} = \frac{\langle M^{-1/2} S_{(i,j,:)}, M^{-1/2} t \rangle}{\|M^{-1/2} S_{(i,j,:)}\| \cdot \|M^{-1/2} t\|}, \quad (8)$$

where (i, j) represents the pixel location of feature maps S to be detected. $\cos_{(i,j)}^{\wedge}$ is the spectral angle cosine similarity between the spectrum of the object t and feature map S . With the cosine similarity, the influence of background clutter is released and the performance of object detection can be improved.

2) Spectral angle awareness branch. Inspired by the spectral angle calculation used to assess depth similarity between pixels, the spectral angle awareness module is proposed. The structure of SAAM is shown in Figure 5. To improve upon the existing formulation, we have reformulated Equation (8) and presented a simplified formula for computing similarity in the SAM. This simplified formula allows for a more efficient and effective calculation, which is formulated as follows:

$$\cos_{(i,j)} \theta = \frac{\langle f(z)_{(i,j,:)}, f(x)_{(i,j,:)} \rangle}{\|f(z)_{(i,j,:)}\| \cdot \|f(x)_{(i,j,:)}\|}, \quad (9)$$

where z and x represent TI and SI of the HS modality. $f(z)$, $f(x)$ are the feature maps extracted by the same f , which is a series of feature extraction and regularization functions. Here, f represents the feature extraction network $S^2\text{FB}$. Indeed, the cosine similarity is calculated by taking the dot product of the mapped HS feature vectors and normalizing it by the magnitude of each vector. In the field of HS tracking, both the classification and localization heads rely on region-level similarity assessments to make their predictions. The features of the TI and SI extracted by the tracker are denoted as $f(z)$ and $f(x)$, respectively. To perform similarity assessments, the

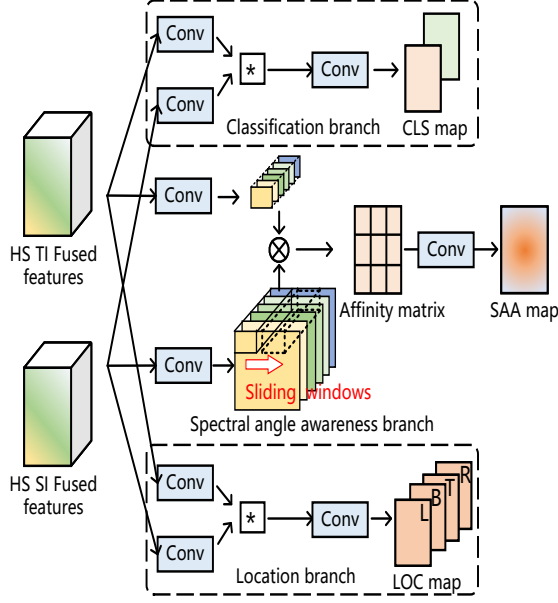


Fig. 5. The architecture of the SAAM includes the CLS branch, LOC branch, and SAA branch.

feature map $f(x)$ undergoes depth-wise separable convolutions using $f(z)$ as the convolution kernel. This operation is represented by the following formula:

$$Sim = f(z) * f(x), \quad (10)$$

where $*$ represents depth-wise cross-correlation layer [36]. It can be seen as an extended region-level version of the SAM, all of which aim to obtain similarity through vector operations. The idea of spectral angle can seamlessly integrate into the tracking prediction head. To achieve this integration, an embedding layer is employed to project the feature maps $f(z)$ and $f(x)$ onto a subspace. This subspace projection enables the calculation of cosine similarity between the two feature maps. It is formulated by:

$$\begin{aligned} f_z^{embed} &= E_z(f(z)), \\ f_x^{embed} &= E_x(f(x)), \end{aligned} \quad (11)$$

where E_z and E_x denote the embedding layers used by $f(z)$ and $f(x)$, respectively. The embedded feature f_z^{embed} is utilized as a sliding convolution kernel to convolve with f_x^{embed} , thereby generating the output map. Consequently, this procedure facilitates the calculation of the region-level affinity matrix between f_z^{embed} and f_x^{embed} . Subsequently, a predicted map of spectral angular affinity M_{SAA} is derived using a 1×1 convolutional layer. The detailed formula is presented as:

$$M_{SAA} = CV2D_{1 \times 1}(Sim(f_z^{embed}, f_x^{embed})), \quad (12)$$

where Sim denotes the 2-D convolutional calculation, and $CV2D_{1 \times 1}$ denotes the 1×1 convolutional layer.

To train the SAAM more effectively, the SAAL is proposed. The positive and negative sample regions as [21] are constructed to transfer the triplet optimization [39] to the HS

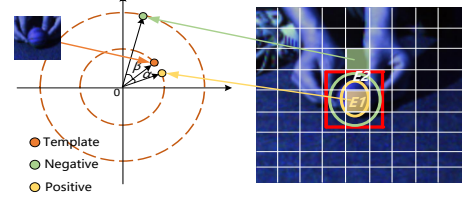


Fig. 6. The architecture of the SAAL. During optimization, the similarity of positive sample pairs learned by the network increases, while the similarity of negative sample pairs decreases.

tracking. The core idea behind triplet loss is to take three data samples at a time, typically referred to as an “anchor”, a “positive”, and a “negative”. The anchor and positive samples belong to the same class or depict the same object, while the negative samples come from a different class. Therefore, the SAAL is designed to maximize the similarity between the anchor and the positive while minimizing the similarity between the anchor and the negative. As shown in Figure 6, the ground-truth bounding box of SI is marked with the red box, we construct two ellipses $E1$ and $E2$. The position (i, j) inside $E1$ is marked as positive p , and the position (i, j) outside $E2$ is marked as negative n . We use the features of TI extracted by the tracker as anchors to form positive pairs with positive regions in SI and negative pairs with negative regions in SI. The SAAL is formulated by:

$$L_{SAAL} = \sum_{\substack{p \in E1 \\ n \in \mathbb{C}(E2)}} [Sim(a, p) - Sim(a, n)], \quad (13)$$

where $p \in E1$ denotes the point inside $E1$ of the M_{SAA} , and $n \in \mathbb{C}(E2)$ denote the complementary point of $E2$, i.e., outside $E2$. a denotes the template image. $Sim(a, p)$ and $Sim(a, n)$ denote the cosine similarities of positive pairs and negative pairs, respectively. During the optimization process, the network learns to increase the similarity between positive sample pairs, while decreasing the similarity between negative sample pairs. This means that the angle between the feature vectors of positive sample pairs in the feature space becomes smaller, while the angle between the feature vectors of negative sample pairs becomes larger. This intuitive understanding is illustrated in Figure 1(c). During inference, SAAM assists the trackers in enhancing the response of objects within TI as it appears in SI. This enhancement facilitates the precise localization of the object within the region of similarity shared between TI and SI.

3) Classification and location branch. The classification and location heads are widely used to predict the location and size of objects [21]. The former outputs the CLS map $M_{CLS} \in \mathbb{R}^{H \times W \times 2}$ to estimate whether the pixels belong to targets or background, and the latter outputs the four-channel LOC map $M_{LOC} \in \mathbb{R}^{H \times W \times 4}$ to calculate the offset from the predicted location to four sides to ground-truth box. To train the SSF-Net effectively, we employ a combination of the SAAL, cross-entropy loss, and the intersection over union (IOU) loss [40]. This joint training approach allows the network to optimize both the classification and localization

performance. The SAAL is incorporated to enhance the learning of spectral angle awareness, while the cross-entropy loss and the IOU loss contribute to the overall training objective. It is formulated as:

$$L = \alpha L_{CLS} + \beta L_{LOC} + \gamma L_{SAAL}, \quad (14)$$

where α , β , and γ denote the trade-off parameters. Here, we empirically set $\alpha = 1$, $\beta = 2$, and $\gamma = 1$ for all experiments. Then, to ensemble the prediction from HS and RGB modalities, a weighted prediction method is adopted to learn the weights of the two modalities in a self-adaptive way. The weighted fusion prediction M_{CLS} and M_{LOC} are obtained from:

$$\begin{aligned} M_{CLS} &= \lambda_1 M_{CLS}^{HS} + \lambda_2 M_{CLS}^{RGB}, \\ M_{LOC} &= \lambda_1 M_{LOC}^{HS} + \lambda_2 M_{LOC}^{RGB}, \end{aligned} \quad (15)$$

where λ_1 and λ_2 denote the trainable parameters, respectively. With the weighted prediction, the CLS and LOC maps integrate the information from two branches, thereby enhancing the accuracy of object localization. Finally, considering the widespread utilization of ensemble prediction in existing methods, we aggregate the prediction maps from the final three stages of both the RGB and HS backbone networks. Furthermore, through the joint calculation of the loss function, the proposed method allows for the simultaneous prediction of the class and location of objects during the inference stage. This integrated approach enhances the efficiency and effectiveness of object prediction, providing more accurate and reliable results.

IV. EXPERIMENTS

A. Experiment Settings

Datasets. The HOTC dataset [6] is used to validate the effectiveness of the proposed method. The dataset is divided into a training set comprising 40 videos and a testing set consisting of 35 videos. To capture different objects, both RGB and HS cameras are employed for simultaneous recording, resulting in each video containing three types of modality data: RGB, HS, and a generated false-color image. The HS image cubes within the dataset consist of 16 spectral bands. Furthermore, the dataset contains 11 challenging factors, including background clutter (BC), deformation (DEF), fast motion (FM), illumination variation (IV), in-plane rotation (IPR), low resolution (LR), motion blur (MB), out-of-occlusion (OCC), plane rotation (OPR), out-of-view (OV), and scale variation (SV).

Evaluation Metrics. The area under the curve (AUC) of the success plot and the precision rate at the threshold of 20 pixels, which is denoted as DP_20, are used as the evaluation metrics. The success plots are utilized to assess the Intersection over Union (IOU) between the predicted bounding box and the ground truth. These plots illustrate the proportion of frames exceeding various IOU thresholds by depicting a success curve, with the IOU threshold spanning from 0 to 1. A larger area under the curve (AUC) represents the superior tracking performance. Regarding precision metrics, they gauge the discrepancy in pixels between the centers of the predicted and

ground truth bounding boxes. The precision rate curve is then constructed by plotting the proportion of frames with a center offset below a given threshold, which extends from 0 to 50 pixels. A lower center offset corresponds to enhanced tracking accuracy.

Implementation Details. All experiments are conducted using an NVIDIA RTX 4090 GPU. For the RGB branches, we utilize a pre-trained ResNet-50 network sourced from training on the COCO [41], ImageNet VID [42], and YouTube-BB [43] dataset as the backbone network. The SSF-Net is not initialized with any pre-trained parameters. During the training phase, the parameters of the RGB stream are kept fixed, while only the parameters of the HS stream are subject to training. We set the batch size to 30 and the learning rate is initialized as 0.005, applying a warm-up learning rate adjustment strategy. The weight decay and momentum are configured at 0.0001 and 0.9, respectively.

B. Comparison with State-of-the-arts

In this subsection, we conduct multiple experiments to demonstrate the effectiveness of our method, including performance comparisons with advanced HS trackers, performance comparisons with advanced RGB trackers, attribute-based comparisons, and visualization analysis.

Comparison with HS Trackers. We first compare the proposed SSF-Net with advanced HS trackers, including band regrouping-based methods SEE-Net, BAE-Net, SST-Net, and band aware-based method SPIRIT. BAE-net initially learned spectral weights in the form of channel attention, and it regrouped the HS cubes to multiple three-channel false-color images based on the spectral weight, thereby transferring existing RGB trackers to process HS tracking. SEE-Net learned the weights between bands in the form of an autoencoder. SST-Net built a temporal-aware false-color image generation framework. SPIRIT utilized both channel attention and an autoencoder-like structure for band awareness, while also considering both intra-band and inter-band interactions. It is worth noting that we reproduced SEE-Net and the results of other trackers can be obtained from the corresponding paper.

The experimental results are listed in Table I. With no consideration of HS feature extraction, the performance of BAE-Net using only spectral attention is 0.606 of the AUC score and 0.878 of DP_20. The tracking performance of SST-net, a band regrouping method that considers spatial, spectral, and temporal information simultaneously, can achieve the 0.623 AUC score and 0.917 DP_20, which compensates for the lack of single spectral attention. SEE-Net regroups bands from the perspective of autoencoder, further achieving the performance of 0.654 of AUC score and 0.907 of DP_20. It can be seen that using only the channel attention mechanism or autoencoder-like structures has limited ability in mining band relationships, which yields the general tracking performance. Methods based on band regrouping are not sufficient to extract robust HS features and using existing RGB trackers to infer the modeling of the spectral relationships will limit the performance of HS tracking. By jointly considering the spectral attention mechanism and autoencoder structure, SPIRIT provides more

TABLE I
OVERALL PERFORMANCE COMPARISON OF HS AND VISUAL TRACKER. THE HS TRACKERS DEAL WITH THE HSIS AND THE VISUAL TRACKER RUNS ON THE FALSE-COLOR IMAGES. WE USE THE RED AND BLUE FONTS TO HIGHLIGHT THE TOP TWO VALUES.

Method	HS tracker					Visual tracker			
	SSF-Net	BAE-Net [28]	SEE-Net [11]	SPIRIT [30]	SST-Net [44]	TransT [45]	SiamGAT [20]	SimTrack [46]	OTrack [24]
AUC	0.680	0.606	0.654	0.679	0.623	0.633	0.581	0.599	0.557
DP_20	0.939	0.878	0.907	0.925	0.917	0.879	0.827	0.845	0.815

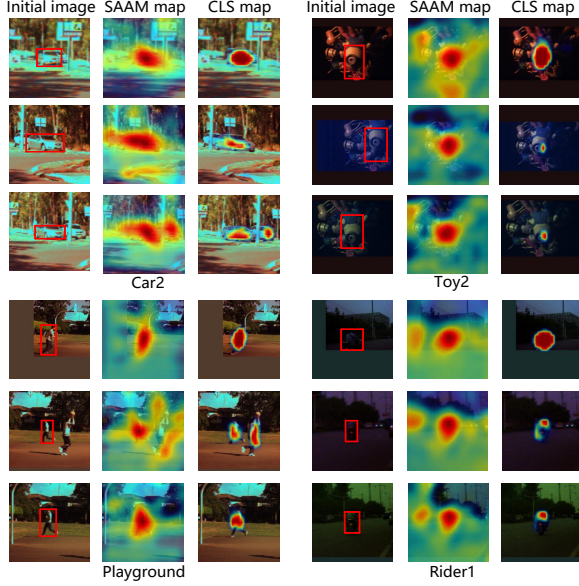


Fig. 7. The visualization of heatmaps on the HOTC dataset. The red color represents high response while the blue color represents low response.

effective tracking results with an AUC score of 0.679 and DP_20 of 0.925. The perception of spectral relationships and the Transformer-based prediction head further improve the performance. Our method not only considers the fusion of spectral and spatial information, but also designs a spectral sensing module for tracking and prediction, and the experimental results achieve the best, with the AUC score of 0.680 and DP_20 of 0.939. This proves the effectiveness of SSF-Net, where S^2 FB and SAFM can extract more discriminative features, while SAAM can more accurately predict the position of objects.

Comparison with RGB Trackers. In addition, we also compare the SSF-Net with advanced RGB trackers, including SiamGAT, OTrack, SimTrack, and TransT. The false-color images of the HOTC dataset are used to perform experiments. As shown in Table I, the SSF-Net provides better performance compared with the RGB tracker. Due to the difficulty in handling factors such as lighting changes and background interference, the RGB trackers are generally weaker than HS trackers in performance, indicating the advantages of HS data in processing challenging scenes.

Visualization Analysis. To better demonstrate the performance of our tracker and the effectiveness of the proposed SAAM and SAAL, we conduct several visualization experiments in this section.

1) **Heatmap Visualization.** To demonstrate the effectiveness

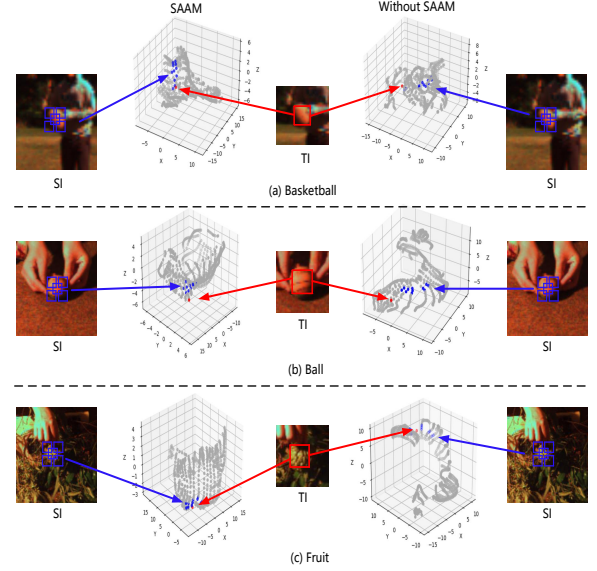


Fig. 8. The feature distribution visualization of SAAL. The red points denote the TI samples and the blue and gray points denote the positive and negative SI samples.

of our proposed SAAM intuitively, we utilize the Grad-CAM++ [47] for feature visualization of classification heads and SAAM. The brighter the color, the higher the level of attention received by the network, which reflects the contribution of tracking performance in this region. The four scenarios are selected including *car2*, *toy2*, *playground* and *rider1*. The experimental results are shown in Figure 7. The first and fourth columns are the original images. The ground-truth bounding box is framed by red lines. The second and fifth columns are SAA maps and the third and sixth columns are CLS maps. The brighter the color, the higher attention received by the network, reflecting the contribution of tracking performance in this region. Due to the visually similar cars and people in the *car2* and *playground* scenes, traditional CLS prediction heads may be confused with tracking objects, as shown in the CLS map of *car2* in the third line and the CLS map of *playground* in the second line. The prediction head also responds to similar objects that appear, which may be detrimental to improving tracking performance. The SAAM focuses on spectral similarity calculation, which can handle the problem of similar appearances of different objects. We can see that although SAAM also responds to other similar objects, such as the SAA map of *car2* in the third row and the SAA map of *playground* in the second row, the area with the highest response is still the tracking object, reflecting the robustness of the SAAM algorithm in handling similar objects.

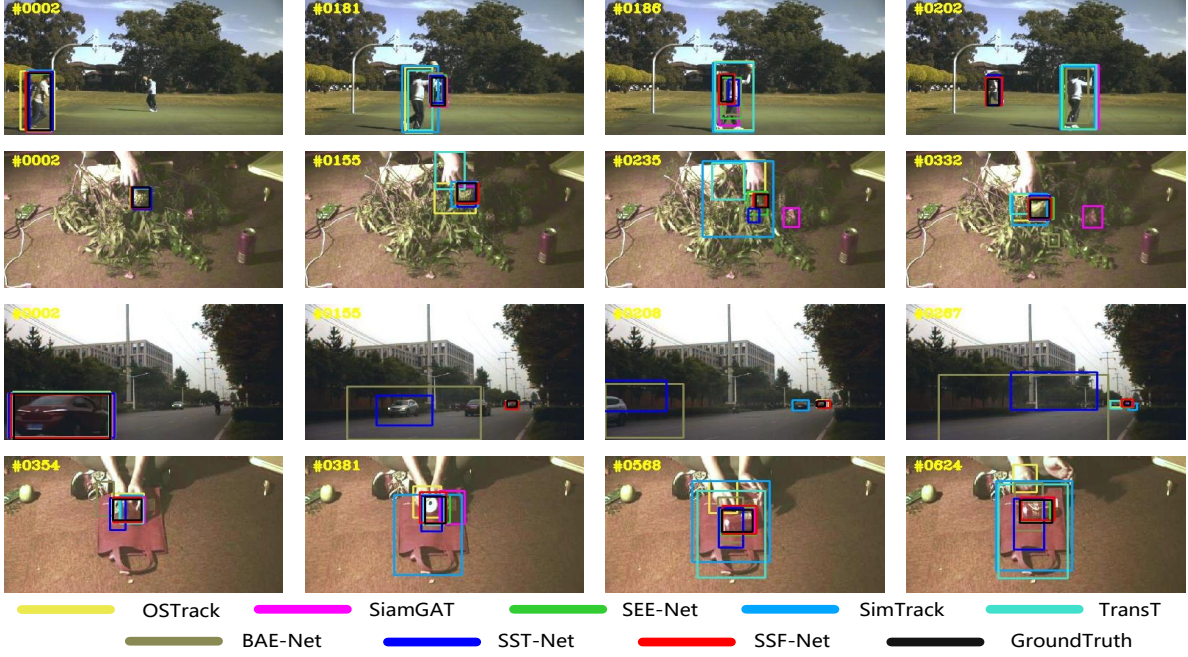


Fig. 9. Tracking results on the false-color images of *playground*, *forest*, *car3*, and *coke* scenarios.

In addition, it can be seen from *toy2* and *rider1* scenarios that SAAM has a large receptive field and can perceive complete objects, avoiding the local overfitting of objects.

2) *Feature Distribution Comparison*. To prove the validity of our proposed SAAL, we also select frames from three different clips and use the *t*-SNE methods to visualize the spectral features of TI and different region features of SI. The results are shown in Figure 8. The blue box in SI represents the area to be detected where the tracked object appears, while the red box in TI represents the object to be tracked, corresponding to blue and red points in the feature space, respectively. Local features that do not belong to the area to be detected are represented by gray points. After training with SAAL, the TI and SI samples can come closer in the feature space. With the proposed SAAL, the tracker can achieve better similarity modeling ability and correctly detect the object to be tracked.

3) *Tracking Results*. We select videos from four different scenarios, including *playground*, *forest*, *car3*, and *coke* to show the visualization results of advanced RGB and HS trackers. The result is shown in Figure 9. The ground-truth bounding box is framed by black lines. The subsequent tracking results are obtained from the first frames based on the positions of labels, which are shown from the second column to the fourth column. Firstly, for *playground* scenes where occlusion is the main challenge, both the HS tracker and RGB tracker are susceptible to visual interference from similar objects, for example, frames 181 and 188, resulting in incorrect objects. Our proposed SSF-Net, due to its focus on the similarity between bands, has robustness in processing visually similar objects and can effectively solve the occlusion problem of similar objects. Then, we can also see from the scene of *car3* that most trackers struggle to handle the scale changes

of objects, especially for tracking small objects. SSF-Net can extract more spectral information, ensuring feature integrity in the event of visual information loss, thereby maintaining tracking performance. In addition, the results of *fruit* and *coke* scenes also show the effectiveness of SSF-Net in dealing with object rotation and background clutter.

Attribute-Based Comparison. To demonstrate the ability to handle the challenging factors of SSF-Net, Figure 10 shows the success plot results of 11 attribute-based experiments. It can be observed that the SSF-Net achieved the top two results in 10 out of 11 scenarios. Among them, SSF-Net performs significantly better than other trackers in scenarios where spatial information is disrupted, such as BC, SV, FM, LR, DEF, and MB, which shows the robustness of the algorithm equipped with SAAM against visual interference. Due to the fusion of spectral and visual information, the SSF-Net can respond to objects in a transient occlusion state and therefore has superior performance in scenarios such as OCC and IV. For the two rotating scenes of IPR and OPR, although the visual features of the object have changed, the HS tracker can extract spectral features. In particular, SSF-Net captures the object based on spectral similarity, thus having better performance. However, the performance of SSF-Net in OV is poor because the algorithm is difficult to propose robust features for objects beyond the receptive field, and cannot integrate spectral and spatial information. Nevertheless, SSF-Net still achieves an overall performance of 0.680 AUC score and 0.939 DP₂₀, which demonstrates the effectiveness of the proposed methods.

C. Ablation Experiments

In this subsection, to evaluate the effectiveness of our methods, several ablation experiments are conducted.

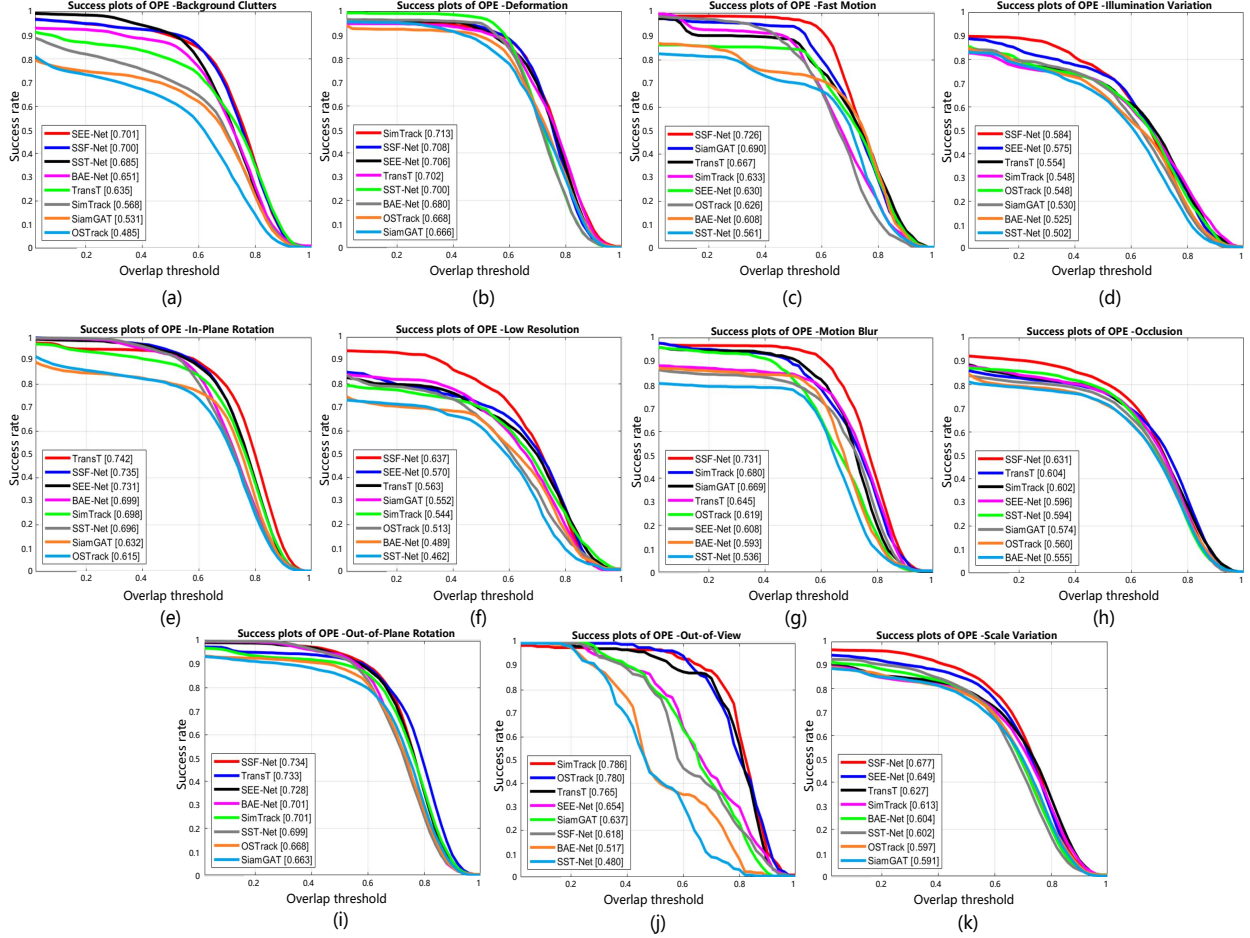


Fig. 10. Attribute-based comparison of success plots. (a) Success plot of background clutters (BC). (b) Success plot of deformation (DEF). (c) Success plot of fast motion (FM). (d) Success plot of illustration Variation (IV). (e) Success plot of in-plane rotation (IPR). (f) Success plot of low resolution (LR). (g) Success plot of motion blur (MB). (h) Success plot of occlusion (OCC). (i) Success plot of out-of-plane clutters (OPR). (j) Success plot of out-of-view (OV). (k) Success plot of scale variation (SV).

Evaluation of Each Component. Firstly, we reproduce the bi-stream ResNet-50 network proposed by Liu *et al.* [12] as the baseline, which is marked as “B”. Then, we replace the ResNet-50 network of HS stream with S^2 FB, which is annotated as “S”, and conduct experiments under the same fusion module SSATTN [12]. The experimental results are listed in Table II. Compared with the baseline model, S^2 FB improves the AUC score by 0.012 and DP_20 by 0.008. Then, based on “S”, we replace SSATTN with SAFM to demonstrate the superiority of SAFM in intra-modality and cross-modality spectral attention, which is denoted as “F”. The AUC score yields 0.675 and DP_20 yields 0.934, demonstrating the effectiveness of SAFM. Furthermore, The SAAM is incorporated into “F”, which is annotated as “A”, and the SAAL is used for training. The experimental results have further improved, yielding an AUC score of 0.680 and DP_20 of 0.939. It demonstrates the effectiveness of S^2 FB in extracting spectral information, the superiority of SAFM over intra-modality attention, and the ability of SAAM to supplement the shortcomings of existing tracking heads in object localization prediction.

Evaluation of Different Backbone Settings. To assess the

TABLE II
ABLATION EXPERIMENTAL RESULTS WITH THE BASELINE MODEL. Δ INDICATES THE AMOUNT OF VARIATION.

Methods	AUC	DP_20	Δ (AUC)	Δ (DP_20)
B	0.661	0.924	-	-
S	0.673	0.932	+0.012	+0.008
S+F	0.675	0.934	+0.014	+0.010
S+F+A	0.680	0.939	+0.019	+0.015

TABLE III
ABLATION EXPERIMENTAL RESULTS WITH THE BASELINE MODEL. Δ INDICATES THE AMOUNT OF VARIATION COMPARED WITH THE RESULTS OF THE FIRST LINE.

Methods	AUC	DP_20	Δ (AUC)	Δ (DP_20)
without res	0.647	0.896	-	-
res	0.673	0.932	+0.026	+0.036
spatial	0.470	0.786	-0.177	-0.110
spectral	0.658	0.913	+0.110	+0.017
both	0.675	0.934	+0.028	+0.038

impact of varying backbone architectures, we conduct experiments with the individual spatial and spectral branches of the S^2 FB, and removing the residual components. The

TABLE IV

ABLATION EXPERIMENTAL RESULTS OF DIFFERENT FUSION METHODS. Δ INDICATES THE AMOUNT OF VARIATION COMPARED WITH THE RESULTS OF THE FIRST LINE.

Methods	AUC	DP_20	Δ (AUC)	Δ (DP_20)
SAFM	0.675	0.934	-	-
ADD	0.636	0.888	-0.039	-0.044
CONCAT	0.662	0.926	-0.013	-0.008
SE-Net [48]	0.665	0.930	-0.010	-0.004
SaE-Net [49]	0.670	0.927	-0.005	-0.007
ECA-Net [35]	0.673	0.932	-0.002	-0.002

TABLE V

ABLATION EXPERIMENTAL RESULTS OF DIFFERENT PREDICTION STRATEGY. Δ INDICATES THE AMOUNT OF VARIATION COMPARED WITH THE RESULTS OF THE FIRST LINE.

Methods	AUC	DP_20	Δ (AUC)	Δ (DP_20)
weighted prediction	0.680	0.939	-	-
average prediction	0.639	0.915	-0.041	-0.024
HS prediction	0.230	0.510	-0.450	-0.429
RGB prediction	0.623	0.871	-0.057	-0.068

experimental results are listed in Table III. We first verify the effectiveness of the residual structure, and the experimental results achieve 0.673 of the AUC score and 0.932 of DP_20, which shows the importance of residual structure. Next, we explore the branches independently for feature extraction. The spatial branch, solely based on depthwise separable convolutions, lacks comprehensive channel information, resulting in a lower AUC score and DP_20 of 0.470 and 0.786, respectively. Meanwhile, the spectral branch alone achieved an AUC score of 0.658 and a DP_20 of 0.913, illustrating that while effective, the performance of each branch is not as robust as when combined. When conducting experiments with the complete S^2 FB structure, the model performance achieved the AUC score of 0.675 and DP_20 of 0.934, respectively. It demonstrates that the integrated approach of S^2 FB to capturing both spatial and spectral information offers a more comprehensive feature representation, thereby confirming the effectiveness of the proposed S^2 FB.

Evaluation of Different Fusion Methods. The feature fusion is a key aspect of cross-modality tracking. To show the effectiveness of our proposed SAFM, we conduct experiments with various fusion methods, including element-wise addition (ADD), concatenation (CONCAT), and state-of-the-art spectral attention methods including SE-Net [48], SaE-Net [49], and ECA-Net [35]. The results of these experiments are presented in Table IV. The simplest methods, addition, and concatenation, without any attention mechanisms, exhibit the least impressive performance. The current spectral attention mechanisms focus on enhancing within-modality features and fall short in harnessing cross-modality feature interactions. Consequently, the most effective result among them is achieved by ECA-Net, yielding the AUC score and DP_20 of 0.673 and 0.932, respectively. However, these scores are still 0.2% lower than those achieved by SAFM. Such a comparison shows the advantages of SAFM in the context of feature fusion, confirming that our module not only refines intra-modality representation but also effectively captures and leverages the interrelations across modalities.

Evaluation of Different Prediction Strategy. In this section, we evaluate the performance of our weighted prediction approach. Drawing upon the “S” model configuration, we compare four different prediction strategies: using the HS branch alone, using the RGB branch alone, averaging the predictions from both, and applying a weighted prediction method. Experimental results are listed in Table V. It can be seen that using the HS branch to predict only achieves the AUC score of 0.230 and DP_20 of 0.510. This was expected, as the S^2 FB is initially trained from scratch on the HOTC dataset, making it challenging for the HS branch alone to develop robust feature extraction capabilities. Then, the result of the RGB branch is 0.623 of the AUC score and DP_20 of 0.871. Due to the parameter freezing of the RGB branch, only the knowledge of the RGB domain is used for false-color image tracking, resulting in poor tracking performance. For average prediction, although the prediction results of both modalities are comprehensively considered, the tracking performance reached an AUC score of 0.639 and DP_20 of 0.915. However, in different scenarios, the contributions of HS and RGB modality to the results should be different. So we used the weighted prediction method to adjust the weights of the two modality predictions adaptively, and the final results are the AUC score of 0.680 and DP_20 of 0.939. This further shows the effectiveness of the weighted prediction method.

V. CONCLUSION

In this article, we proposed a spatial-spectral fusion network with spectral angle awareness (SSF-Net) for hyperspectral object tracking. We first designed spatial-spectral feature backbone S^2 FB to extract the more robust spatial and spectral features compared with the state-of-the-art trackers. Then, a spectral attention fusion module (SAFM) was proposed to incorporate the visual information from the RGB modality into the HS modality to obtain robust HS fusion features. Finally, a spectral angle awareness module (SAAM) was designed to predict the more accurate position of objects. With the proposed spectral angle awareness loss (SAAL), the tracker can be trained in an end-to-end way. Experimental results on the HOTC dataset showed the effectiveness of our proposed methods.

REFERENCES

- [1] K.-H. Lee and J.-N. Hwang, “On-road pedestrian tracking across multiple driving recorders,” *IEEE Trans. on Multimedia*, vol. 17, no. 9, pp. 1429–1438, 2015.
- [2] S. Chandra, G. Sharma, S. Malhotra, D. Jha, and A. P. Mittal, “Eye tracking based human computer interaction: Applications and their uses,” in *2015 International Conference on Man and Machine Interfacing (MAMI)*. IEEE, 2015, pp. 1–5.
- [3] X. Tian, J. Liu, M. Mallick, and K. Huang, “Simultaneous detection and tracking of moving-target shadows in visar imagery,” *IEEE Trans. on Geoscience and Remote Sensing*, vol. 59, no. 2, pp. 1182–1199, 2020.
- [4] J. He, Q. Yuan, J. Li, Y. Xiao, D. Liu, H. Shen, and L. Zhang, “Spectral super-resolution meets deep learning: Achievements and challenges,” *Information Fusion*, p. 101812, 2023.
- [5] Y. Tang, Y. Liu, and H. Huang, “Target-aware and spatial-spectral discriminant feature joint correlation filters for hyperspectral video object tracking,” *Computer Vision and Image Understanding*, vol. 223, p. 103535, 2022.

- [6] F. Xiong, J. Zhou, and Y. Qian, "Material based object tracking in hyperspectral videos," *IEEE Trans. on Image Processing*, vol. 29, pp. 3719–3733, 2020.
- [7] Z. Hou, W. Li, J. Zhou, and R. Tao, "Spatial-spectral weighted and regularized tensor sparse correlation filter for object tracking in hyperspectral videos," *IEEE Trans. on Geoscience and Remote Sensing*, vol. 60, pp. 1–12, 2022.
- [8] E. Ouyang, J. Wu, B. Li, L. Zhao, and W. Hu, "Band regrouping and response-level fusion for end-to-end hyperspectral object tracking," *IEEE Geoscience and Remote Sensing Letters*, vol. 19, pp. 1–5, 2021.
- [9] C. Sun, X. Wang, Z. Liu, Y. Wan, L. Zhang, and Y. Zhong, "Siamohot: A lightweight dual siamese network for onboard hyperspectral object tracking via joint spatial-spectral knowledge distillation," *IEEE Transactions on Geoscience and Remote Sensing*, vol. 61, pp. 1–12, 2023.
- [10] L. Gao, P. Liu, Y. Jiang, W. Xie, J. Lei, Y. Li, and Q. Du, "Cbff-net: A new framework for efficient and accurate hyperspectral object tracking," *IEEE Trans. on Geoscience and Remote Sensing*, vol. 61, pp. 1–14, 2023.
- [11] Z. Li, F. Xiong, J. Zhou, J. Lu, and Y. Qian, "Learning a deep ensemble network with band importance for hyperspectral object tracking," *IEEE Trans. on Image Processing*, vol. 32, pp. 2901–2914, 2023.
- [12] Z. Liu, X. Wang, Y. Zhong, M. Shu, and C. Sun, "Siamhyper: Learning a hyperspectral object tracker from an rgb-based tracker," *IEEE Trans. on Image Processing*, vol. 31, pp. 7116–7129, 2022.
- [13] C. Zhao, H. Liu, N. Su, and Y. Yan, "Tftn: A transformer-based fusion tracking framework of hyperspectral and rgb," *IEEE Trans. on Geoscience and Remote Sensing*, vol. 60, pp. 1–15, 2022.
- [14] H. Ye, H. Liu, F. Meng, and X. Li, "Bi-directional exponential angular triplet loss for rgb-infrared person re-identification," *IEEE Transactions on Image Processing*, vol. 30, pp. 1583–1595, 2020.
- [15] F. A. Kruse, A. Lefkoff, J. Boardman, K. Heidebrecht, A. Shapiro, P. Barloon, and A. Goetz, "The spectral image processing system (sips)—interactive visualization and analysis of imaging spectrometer data," *Remote Sensing of Environment*, vol. 44, no. 2-3, pp. 145–163, 1993.
- [16] L. Bertinetto, J. Valmadre, J. F. Henriques, A. Vedaldi, and P. H. Torr, "Fully-convolutional siamese networks for object tracking," in *European Conf. on Computer Vision*. Springer, 2016, pp. 850–865.
- [17] F. Xie, C. Wang, G. Wang, Y. Cao, W. Yang, and W. Zeng, "Correlation-aware deep tracking," in *Proceedings of the IEEE/CVF Conference on Computer Vision and Pattern Recognition*, 2022, pp. 8751–8760.
- [18] M. Paul, M. Danelljan, C. Mayer, and L. Van Gool, "Robust visual tracking by segmentation," in *European Conf. on Computer Vision*. Springer, 2022, pp. 571–588.
- [19] B. Li, J. Yan, W. Wu, Z. Zhu, and X. Hu, "High performance visual tracking with siamese region proposal network," in *Proceedings of the IEEE Conf. on Computer Vision and Pattern Recognition*, 2018, pp. 8971–8980.
- [20] D. Guo, Y. Shao, Y. Cui, Z. Wang, L. Zhang, and C. Shen, "Graph attention tracking," in *Proceedings of the IEEE/CVF Conf. on Computer Vision and Pattern Recognition*, 2021, pp. 9543–9552.
- [21] Z. Chen, B. Zhong, G. Li, S. Zhang, and R. Ji, "Siamese box adaptive network for visual tracking," in *Proceedings of the IEEE/CVF Conf. on Computer Vision and Pattern Recognition*, 2020, pp. 6668–6677.
- [22] N. Wang, W. Zhou, J. Wang, and H. Li, "Transformer meets tracker: Exploiting temporal context for robust visual tracking," in *Proceedings of the IEEE/CVF Conference on Computer Vision and Pattern Recognition*, 2021, pp. 1571–1580.
- [23] P. Sun, J. Cao, Y. Jiang, R. Zhang, E. Xie, Z. Yuan, C. Wang, and P. Luo, "Transtrack: Multiple object tracking with transformer," *arXiv preprint arXiv:2012.15460*, 2020.
- [24] B. Ye, H. Chang, B. Ma, S. Shan, and X. Chen, "Joint feature learning and relation modeling for tracking: A one-stream framework," in *European Conf. on Computer Vision*. Springer, 2022, pp. 341–357.
- [25] J. Zhu, S. Lai, X. Chen, D. Wang, and H. Lu, "Visual prompt multi-modal tracking," in *Proceedings of the IEEE/CVF Conference on Computer Vision and Pattern Recognition*, 2023, pp. 9516–9526.
- [26] H. Van Nguyen, A. Banerjee, and R. Chellappa, "Tracking via object reflectance using a hyperspectral video camera," in *2010 IEEE Computer Society Conf. on Computer Vision and Pattern Recognition-Workshops*. IEEE, 2010, pp. 44–51.
- [27] B. Uzkent, A. Rangnekar, and M. J. Hoffman, "Tracking in aerial hyperspectral videos using deep kernelized correlation filters," *IEEE Transactions on Geoscience and Remote Sensing*, vol. 57, no. 1, pp. 449–461, 2018.
- [28] Z. Li, F. Xiong, J. Zhou, J. Wang, J. Lu, and Y. Qian, "Bae-net: A band attention aware ensemble network for hyperspectral object tracking," in *2020 IEEE International Conf. on Image Processing (ICIP)*. IEEE, 2020, pp. 2106–2110.
- [29] W. Li, Z. Hou, J. Zhou, and R. Tao, "Siambag: Band attention grouping-based siamese object tracking network for hyperspectral videos," *IEEE Trans. on Geoscience and Remote Sensing*, 2023.
- [30] Y. Chen, Q. Yuan, Y. Tang, Y. Xiao, J. He, and L. Zhang, "Spirit: Spectral awareness interaction network with dynamic template for hyperspectral object tracking," *IEEE Transactions on Geoscience and Remote Sensing*, 2023.
- [31] M. A. Islam, J. Zhou, W. Zhang, and Y. Gao, "Background-aware band selection for object tracking in hyperspectral videos," *IEEE Geoscience and Remote Sensing Letters*, 2023.
- [32] L. Zhang, M. Danelljan, A. Gonzalez-Garcia, J. Van De Weijer, and F. Shahbaz Khan, "Multi-modal fusion for end-to-end rgb-t tracking," in *Proceedings of the IEEE/CVF International Conference on Computer Vision Workshops*, 2019, pp. 0–0.
- [33] P. Zhang, J. Zhao, C. Bo, D. Wang, H. Lu, and X. Yang, "Jointly modeling motion and appearance cues for robust rgb-t tracking," *IEEE Transactions on Image Processing*, vol. 30, pp. 3335–3347, 2021.
- [34] X. Lan, W. Zhang, S. Zhang, D. K. Jain, and H. Zhou, "Robust multi-modality anchor graph-based label prediction for rgb-infrared tracking," *IEEE Transactions on Industrial Informatics*, 2019.
- [35] Q. Wang, B. Wu, P. Zhu, P. Li, W. Zuo, and Q. Hu, "Eca-net: Efficient channel attention for deep convolutional neural networks," in *Proceedings of the IEEE/CVF Conference on Computer Vision and Pattern Recognition*, 2020, pp. 11 534–11 542.
- [36] B. Li, W. Wu, Q. Wang, F. Zhang, J. Xing, and J. Yan, "Siamrpn++: Evolution of siamese visual tracking with very deep networks," in *Proceedings of the IEEE/CVF Conf. on Computer Vision and Pattern Recognition*, 2019, pp. 4282–4291.
- [37] C.-I. Chang, "Hyperspectral target detection: Hypothesis testing, signal-to-noise ratio, and spectral angle theories," *IEEE Transactions on Geoscience and Remote Sensing*, vol. 60, pp. 1–23, 2021.
- [38] J. Zeng and Q. Wang, "Sparse tensor model-based spectral angle detector for hyperspectral target detection," *IEEE Transactions on Geoscience and Remote Sensing*, vol. 60, pp. 1–15, 2022.
- [39] A. Hermans, L. Beyer, and B. Leibe, "In defense of the triplet loss for person re-identification," *arXiv preprint arXiv:1703.07737*, 2017.
- [40] J. Yu, Y. Jiang, Z. Wang, Z. Cao, and T. Huang, "Unitbox: An advanced object detection network," in *Proceedings of the 24th ACM International Conf. on Multimedia*, 2016, pp. 516–520.
- [41] T.-Y. Lin, M. Maire, S. Belongie, J. Hays, P. Perona, D. Ramanan, P. Dollár, and C. L. Zitnick, "Microsoft coco: Common objects in context," in *European Conf. on Computer Vision*. Springer, 2014, pp. 740–755.
- [42] O. Russakovsky, J. Deng, H. Su, J. Krause, S. Satheesh, S. Ma, Z. Huang, A. Karpathy, A. Khosla, M. Bernstein *et al.*, "Imagenet large scale visual recognition challenge," *International Journal of Computer Vision*, vol. 115, pp. 211–252, 2015.
- [43] E. Real, J. Shlens, S. Mazzocchi, X. Pan, and V. Vanhoucke, "Youtube-boundingboxes: A large high-precision human-annotated data set for object detection in video," in *proceedings of the IEEE Conf. on Computer Vision and Pattern Recognition*, 2017, pp. 5296–5305.
- [44] Z. Li, X. Ye, F. Xiong, J. Lu, J. Zhou, and Y. Qian, "Spectral-spatial-temporal attention network for hyperspectral tracking," in *2021 11th Workshop on Hyperspectral Imaging and Signal Processing: Evolution in Remote Sensing (WHISPERS)*. IEEE, 2021, pp. 1–5.
- [45] X. Chen, B. Yan, J. Zhu, D. Wang, X. Yang, and H. Lu, "Transformer tracking," in *Proceedings of the IEEE/CVF Conf. on Computer Vision and Pattern Recognition*, 2021, pp. 8126–8135.
- [46] B. Chen, P. Li, L. Bai, L. Qiao, Q. Shen, B. Li, W. Gan, W. Wu, and W. Ouyang, "Backbone is all you need: A simplified architecture for visual object tracking," in *European Conf. on Computer Vision*. Springer, 2022, pp. 375–392.
- [47] Z. Chen, V. Badrinarayanan, C.-Y. Lee, and A. Rabinovich, "Gradnorm: Gradient normalization for adaptive loss balancing in deep multitask networks," in *International Conference on Machine Learning*. PMLR, 2018, pp. 794–803.
- [48] J. Hu, L. Shen, and G. Sun, "Squeeze-and-excitation networks," in *Proceedings of the IEEE/CVF Conference on Computer Vision and Pattern Recognition*, 2018, pp. 7132–7141.
- [49] M. Narayanan, "Senetv2: Aggregated dense layer for channelwise and global representations," *arXiv preprint arXiv:2311.10807*, 2023.